Journal of Dynamics, Monitoring and Diagnostics, 2023, 2, 262-274
https://doi.org/10.37965/jdmd.2023.186

ISTP
RESEARCH ARTICLE

An Improved Coupled Dynamic Modelling for Exploring Gearbox Vibrations Considering Local Defects

Yaoyao Han,[1,2] Xiaohui Chen,[1,2] Jiawei Xiao,[1,2] James Xi Gu,[3] and Minmin Xu[1,2]
[1]State Key Laboratory of Mechanical Transmission, Chongqing University, Chongqing, China
[2]College of Mechanical and Vehicle Engineering, Chongqing University, Chongqing, China
[3]School of Engineering, University of Bolton, Bolton, BL3 5AB, UK

(Received 03 March 2023; Revised 21 June 2023; Accepted 21 July 2023; Published online 26 July 2023)

Abstract: Gearbox is a key part in machinery, in which gear, shaft and bearing operate together to transmit motion and power. The wide usage and high failure rate of gearbox make it attract much attention on its health monitoring and fault diagnosis. Dynamic modelling can study the mechanism under different faults and provide theoretical foundation for fault detection. However, current commonly used gear dynamic model usually neglects the influence of bearing and shaft, resulting in incomplete understanding of gearbox fault diagnosis especially under the effect of local defects on gear and shaft. To address this problem, an improved gear-shaft-bearing-housing dynamic model is proposed to reveal the vibration mechanism and responses considering shaft whirling and gear local defects. Firstly, an eighteen degree-of-freedom gearbox dynamic model is proposed, taking into account the interaction among gear, bearing and shaft. Secondly, the dynamic model is iteratively solved. Then, vibration responses are expounded and analysed considering gear spalling and shaft crack. Numerical results show that the gear mesh frequency and its harmonics have higher amplitude through the spectrum. Vibration RMS and the shaft rotating frequency increase with the spalling size and shaft crack angle in general. An experiment is designed to verify the rationality of the proposed gearbox model. Lastly, comprehensive analysis under different spalling size and shaft crack angle are analysed. Results show that when spalling size and crack angle are larger, RMS and the amplitude of shaft rotating frequency will not increase linearly. The dynamic model can accurately simulate the vibration of gear transmission system, which is helpful for gearbox fault diagnosis.

Keywords: coupled gear-shaft-bearing-housing dynamic mode; gearbox; gearbox fault diagnosis; local defects; shaft crack

I. INTRODUCTION

Gear transmission system is a key component in rotating equipment, in which gear and bearing operate together to transmit motion and power. Gearbox has been widely used in CNC machine, wind turbine and other fields [1–3]. With the development of mechanical equipment towards complexity and high-power density, the working condition of gearbox has become more complex and tougher. It will lead to local defects on gear or bearing with higher possibility, even the failure of gearbox or machine. If a fault is not detected in time, maintenance activity cannot be organized, which may cause a major accident and economic loss. Hence, gearbox fault diagnosis plays a key role in real production and application.

Vibration signal is usually taken as the preferred source data for fault diagnosis [4]. Especially, in a gearbox system, the acquired vibration data possess rich information of each component, including the motion and coupled effect. Therefore, figuring out the mechanism of the interaction of gear, shaft and bearing in vibration signals is of great significance for gearbox fault diagnosis.

To investigate the dynamic performance of gear transmission systems, Ma *et al.* [5,6] studied the calculation of time-varying mesh stiffness for cracked spur gears. Chen *et al.* [7–9] performed a series of investigations on the dynamic responses of spur gear on tooth root crack, deformation and errors. Wang *et al.* [10] explored the fault mode of gear tooth crack during the process of the propagation for detection through a simulation study. However, in these works, only the vibration responses of gear have been investigated, while the bearing and shaft were neglected. For exploring the dynamic behaviours of the gear transmission systems considering the couple effect of gear and bearing, Sawalhi and Randall [11,12] presented a vibration model to analyse the interaction between the gear and the bearing with 34 degree of freedom (DOF), and vibration responses of bearing local defect were also investigated. However, the interaction mechanism of gear meshing impact on bearing is not clear. Zeng *et al.* [13] studied the vibration response of different positions on gearbox system through finite element method and investigated the relation between the gear meshing stiffness (GMF) and vibration. Hu *et al.* [14] utilized a dynamic model under finite element node to investigate responses of taking a gear-rotor-bearing system at high speed into consideration the time-varying mesh stiffness (TVMS) and other factors. Zhou *et al.* proposed a 16-DOF gear-rotor-bearing dynamic model considering the effect of gear transmission error, bearing clearances and eccentricity. Xiao *et al.* [15] investigated a gear-shaft-bearing-housing dynamic model and analysed impulsive gear mesh force on the vibration characteristics and energy dissipation considering 8 DOF. However, the dynamic gear meshing and local defect were ignored. Fernandez *et al.* [16] investigated the dynamic responses of gear transmission system under the

Corresponding author: Xiaohui Chen (e-mail: chenxiaohui@cqu.edu.cn)

influence of bearing clearance. Chen *et al.* [17] established a geared rotor-bearing system under the effect of gear meshing, shaft and oil film and analysed the vibration characteristics response. Xu *et al.* [18] proposed a coupled nonlinear dynamic model considering gear, shaft and bearing, and vibration characteristics under the influence of bearing clearances were studied. However, the shaft was regarded as rigid in these works.

Overall, it finds that the interaction among gear, shaft and bearing is not explained clearly especially under the effect of gear local defects and shaft deflection. Fatigue and local defects, such as spalling, will appear inevitably on gear surface after long-time operation. The vibration responses of the gear transmission system will show obvious impulses when entering the fault zone. Therefore, the health condition of the gearbox can be detected according to the impulses. However, the diagnostics features of local defects will be affected by distributed faults, such as shaft deflection, resulting in misjudgement on the degree of failure. The coupled effect of gear local defects and shaft deflection on vibration for fault diagnosis is still unclear.

Thus, to fill the gap, this study proposes an improved coupled gear-shaft-bearing-housing dynamic model considering the interaction mechanism among gear, shaft and bearing. Vibration responses when crack appear on gears are investigated. The influence of shaft whirling on vibration is analysed for monitoring gear spalling. The rest part of the paper is organized as follows. Section I expounds the proposed coupled dynamic model. Section II introduces the implementation of the numerical simulation. Section III is the result and analysis. Section IV verifies the improved dynamic model through a gearbox test rig.

II. IMPROVED COUPLED GEARBOX DYNAMIC MODELLING

A. COUPLED DYNAMIC MODEL

An improved dynamic model is established to investigate the vibration response in gear transmission system. The dynamic model is presented in Fig. 1. In this model, gear and bearing connect through a shaft. The gear-bearing-shaft-housing model is given in Equations (1)–(18) [18].

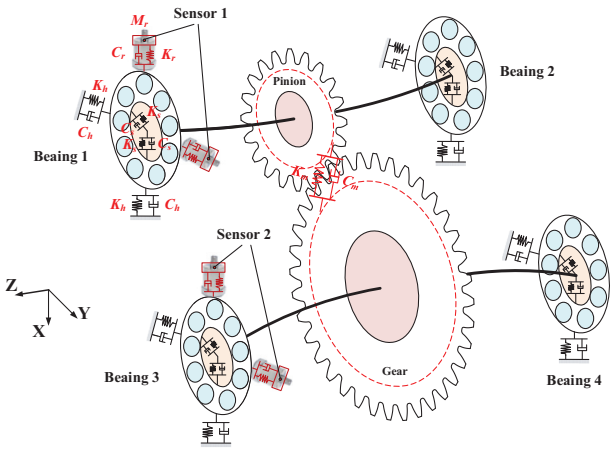

Fig. 1. Schematic diagram of the gear-shaft-bearing-housing dynamic model.

$$M_s\ddot{X}_{s1} + C_{sx}(\dot{X}_p - \dot{X}_{s1}) + K_{sx}(X_p - X_{s1}) + \sum_{i=1}^{N_b} K_{sh}[\delta_{i1}]^{3/2}\cos\phi_{i1} + \sum_{i=1}^{N_b} C_{sh}[v_{i1}]\cos\phi_{i1} = (F_m\cos\alpha)/2, \quad (1)$$

$$M_s\ddot{Y}_{s1} + C_{sy}(\dot{Y}_p - \dot{Y}_{s1}) + K_{sy}(Y_p - Y_{s1}) - \sum_{i=1}^{N_b} K_{sh}[\delta_{i1}]^{3/2}\sin\phi_{i1} + \sum_{i=1}^{N_b} C_{sh}[v_{i1}]\sin\phi_{i1} = (-F_m\sin\alpha)/2, \quad (2)$$

$$M_h\ddot{X}_{h1} + C_h\dot{X}_{h1} + K_hX_{h1} - \sum_{i=1}^{N_b} K_{sh}[\delta_{i1}]^{3/2}\cos\phi_{i1} - \sum_{i=1}^{N_b} C_{sh}[v_{i1}]\cos\phi_{i1} = 0, \quad (3)$$

$$M_h\ddot{Y}_{h_1} + C_h\dot{Y}_{h_1} + K_hY_{h_1} - \sum_{i=1}^{N_b} K_{sh}[\delta_{i1}]^{3/2}\sin\phi_{i1} - \sum_{i=1}^{N_b} C_{sh}[v_{i1}]\sin\phi_{i1} = 0, \quad (4)$$

$$M_r\ddot{X}_{r1} + C_r(\dot{X}_{r1} - \dot{X}_{h1}) + K_r(X_{r1} - X_{h1}) = 0, \quad (5)$$

$$M_r\ddot{Y}_{r1} + C_r(\dot{Y}_{r1} - \dot{Y}_{h1}) + K_r(Y_{r1} - Y_{h1}) = 0, \quad (6)$$

$$M_s\ddot{X}_{s2} + C_s(\dot{X}_g - \dot{X}_{s2}) + K_s(X_g - X_{s_2}) + \sum_{i=1}^{N_b} K_{sh}[\delta_{i2}]^{3/2}\cos\phi_{i2} + \sum_{i=1}^{N_b} C_{sh}[v_{i2}]\cos\phi_{i2} = (-F_m\cos\alpha)/2, \quad (7)$$

$$M_s\ddot{Y}_{s2} + C_s(\dot{Y}_g - \dot{Y}_{s2}) + K_s(Y_g - Y_{s2}) + \sum_{i=1}^{N_b} K_{sh}[\delta_{i2}]^{3/2}\sin\phi_{i2} + \sum_{i=1}^{N_b} C_{sh}[v_{i2}]\sin\phi_{i2} = (-F_m\sin\alpha)/2, \quad (8)$$

$$M_h\ddot{X}_{h_2} + C_h\dot{X}_{h_2} + K_hX_{h_2} - \sum_{i=1}^{N_b} K_{sh}[\delta_{i2}]^{3/2}\cos\phi_{i2} - \sum_{i=1}^{N_b} C_{sh}[v_{i2}]\cos\phi_{i2} = 0, \quad (9)$$

$$M_h\ddot{Y}_{h_2} + C_h\dot{Y}_{h2} + K_hY_{h_2} - \sum_{i=1}^{N_b} K_{sh}[\delta_{i2}]^{3/2}\sin\phi_{i2} - \sum_{i=1}^{N_b} C_{sh}[v_{i2}]\sin\phi_{i2} = 0, \quad (10)$$

$$M_r\ddot{X}_{r2} + C_r(\dot{X}_{r2} - \dot{X}_{h2}) + K_r(X_{r2} - X_{h2}) = 0, \quad (11)$$

$$M_r\ddot{Y}_{r2} + C_r(\dot{Y}_{r2} - \dot{Y}_{h_2}) + K_r(Y_{r2} - Y_{h2}) = 0, \quad (12)$$

$$J_p\ddot{\theta}_p = T_p - M_p, \quad (13)$$

$$J_g\ddot{\theta}_g = T_g - M_g, \quad (14)$$

$$M_p\ddot{X}_p = F_m\cos\alpha - K_{sx}(X_p - X_{s1}) - C_{sx}(\dot{X}_p - \dot{X}_{s1}), \quad (15)$$

$$M_p\ddot{Y}_p = -F_m\sin\alpha - K_{sy}(Y_p - Y_{s1}) - C_{sy}(\dot{Y}_p - \dot{Y}_{s1}), \quad (16)$$

$$M_g\ddot{X}_g = -F_m\cos\alpha - K_s(X_g - X_{s2}) - C_s(\dot{X}_g - \dot{X}_{s2}), \quad (17)$$

$$M_g\ddot{Y}_g = F_m\sin\alpha - K_s(Y_g - Y_{s2}) - C_s(\dot{Y}_g - \dot{Y}_{s2}). \quad (18)$$

where $X_{ij}/\dot{X}_{ij}/\ddot{X}_{ij}$ and $Y_{ij}/\dot{Y}_{ij}/\ddot{Y}_{ij}$ represent the displacement, velocity, acceleration in X and Y direction, respectively. The subscript $i = s,h,r$ indicates shaft, housing and sensors, respectively. The subscript $j = 1,2$ denotes the bearings of shaft 1 and shaft 2, separately. M_i indicates the mass. For gear part, the subscript $i = p,g$ stands for pinion and gear separately. $X_i/\dot{X}_i/\ddot{X}_i$ and $Y_i/\dot{Y}_i/\ddot{Y}_i$ indicate displacement, velocity, acceleration in X and Y direction separately. T_i indicates the applied torque, $\ddot{\theta}_i$ stands for the angular acceleration, α is contact angle. M_{iN} is the normal mesh force moment, J_i represents the moment of inertia of gears, and F_m denotes the gear mesh force. For bearing part, K_s represents stiffness and C_s is damping coefficients of the normal shaft, while $K_{sx,y}$ and $C_{sx,y}$represent stiffness and damping coefficients of the cracked shaft, respectively. K_{sh} means the stiffness and C_{sh} is damping between raceways and rolling elements. Furthermore, δ_{ij} is the deformation and v_{ij} indicates velocity of the i-th ball separately, which can refer to Refs. [4,18,19]. N_b means the number of rolling elements, and ϕ_{ij} denotes the angle position of the i-th ball.

The dynamic gear mesh force and the moment among the gear pair can be calculated through TVMS and damping [18].

$$F_m = K_m\delta_{pg} + C_m v_{pg} \quad (19)$$

$$M_{pN} = F_m \times r_{bp} \quad (20)$$

$$M_{gN} = F_m \times r_{bg} \quad (21)$$

where K_m denotes the TVMS, δ_{pg} is dynamic transmission error, and v_{pg} is its differential coefficient, respectively, C_m stands for the mesh damping, r_{bp} and r_{bg} denote the base radius of pinion and gear separately.

Note that the improved model is constructed based on following considerations and assumptions.

(1) 18 DOF is considered in the dynamic model, which contains the translational motion of inner race, outer race and sensor on vertical (X) and horizontal (Y) direction, the translational motion of pinion and gear on vertical (X) and horizontal (Y) direction and the rotational motion of pinion and gear on axial direction. Therefore, for each bearing, it has 6 DOF. For pinion and gear, they have 6 DOF totally. Other DOF are neglected in this model.

(2) The structure of the model is assumed to be symmetrical. It means that bearing 1 and bearing 2 are assumed to possess the same vibration waveform. Similarly, bearing 3 and bearing 4 are the same.

(3) Geometry and assembly errors except shaft whiling are ignored in this model.

(4) Lubrication, temperature and bearing skidding are ignored in this model.

B. CONTACT STIFFNESS OF NORMAL GEAR

Under the influence of meshing force and torque, gear teeth will be deformed during operation, which mainly includes bending deformation, shear deformation, axial compression deformation, contact deformation and gear fillet-foundation deformation [5–8]. The tooth force diagram of normal gear is shown in Fig. 2.

The bending stiffness, shear stiffness, axial compression stiffness, Hertz contact stiffness and stiffness caused by gear fillet-foundation deflection can be written as [8,18]

$$\frac{1}{K_b} = \int_0^d \frac{(x\cos\alpha_1 - h\sin\alpha_1)^2}{EI_x}dx \quad (22)$$

$$\frac{1}{K_s} = \int_0^d \frac{1.2\cos^2\alpha_1}{GA_x}dx \quad (23)$$

$$\frac{1}{K_a} = \int_0^d \frac{\sin^2\alpha_1}{EA_x}dx \quad (24)$$

$$\frac{1}{K_h} = \frac{4(1-\nu^2)}{\pi Eb} \quad (25)$$

$$\frac{1}{K_f} = \frac{\delta_f}{F} \quad (26)$$

where E is the elastic modulus and G is shearing modulus of gear tooth, and I_x and A_x are the moment of inertia and the area of the section at the distance x from the fixed end of the gear tooth. δ_f represents the fillet-foundation deflection.

According to the geometric relationship between involute tooth profile and rotation angle, Equations (22)–(24) can be transformed to [20]

$$\frac{1}{K_b} = \int_{-\alpha_1}^{\alpha_2} \frac{3\{1+\cos\alpha_1[(\alpha_2-\alpha)\sin\alpha-\cos\alpha]\}^2(\alpha_2-\alpha)\cos\alpha}{2Eb[\sin\alpha+(\alpha_2-\alpha)\cos\alpha]^3}d\alpha \quad (27)$$

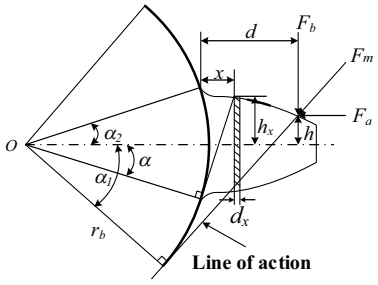

Fig. 2. Tooth force diagram of normal gear.

$$\frac{1}{K_s}=\int_{-\alpha_1}^{\alpha_2}\frac{1.2(1+v)(\alpha_2-\alpha)\cos\alpha\cos^2\alpha_1}{Eb[\sin\alpha+(\alpha_2-\alpha)\cos\alpha]}d\alpha \tag{28}$$

$$\frac{1}{K_a}=\int_{-\alpha_1}^{\alpha_2}\frac{(\alpha_2-\alpha)\cos\alpha\sin^2\alpha_1}{2Eb[\sin\alpha+(\alpha_2-\alpha)\cos\alpha]}d\alpha \tag{29}$$

C. CONTACT STIFFNESS OF FAULTY GEAR

In gearbox, the percentage of gear fault accounts for about 60%, such as spalling and pitting on gear surface. When the tooth surface has spalling fault, the schematic diagram and force analysis of gear tooth meshing is shown in Fig. 3.

The bending stiffness, shearing stiffness and the axial compression stiffness in Fig. 3 can be written as [21]

$$\begin{aligned}\frac{1}{K_b}=&\int_{-\alpha_1}^{\alpha_{h1}}\frac{3\{1+\cos\alpha_1[(\alpha_2-\alpha)\sin\alpha-\cos\alpha]\}^2(\alpha_2-\alpha)\cos\alpha}{2Eb[\sin\alpha+(\alpha_2-\alpha)\cos\alpha]^3}d\alpha\\&+\int_{\alpha_{h1}}^{\alpha_{h2}}\frac{3\{1+\cos\alpha_1[(\alpha_2-\alpha)\sin\alpha-\cos\alpha]\}^2(\alpha_2-\alpha)\cos\alpha}{E(2b-b_s)[\sin\alpha+(\alpha_2-\alpha)\cos\alpha]^3+Eb_s[\sin\alpha+(\alpha_2-\alpha)\cos\alpha-\frac{t_b}{R_{pg}}]^3}d\alpha\\&+\int_{\alpha_{h2}}^{\alpha_2}\frac{3\{1+\cos\alpha_1[(\alpha_2-\alpha)\sin\alpha-\cos\alpha]\}^2(\alpha_2-\alpha)\cos\alpha}{2Eb[\sin\alpha+(\alpha_2-\alpha)\cos\alpha]^3}d\alpha\end{aligned} \tag{30}$$

$$\begin{aligned}\frac{1}{K_s}=&\int_{-\alpha_1}^{\alpha_{h1}}\frac{1.2(1+v)(\alpha_2-\alpha)\cos\alpha\cos^2\alpha_1}{Eb[\sin\alpha+(\alpha_2-\alpha)\cos\alpha]}d\alpha\\&+\int_{\alpha_{h1}}^{\alpha_{h2}}\frac{2.4(1+v)(\alpha_2-\alpha)\cos\alpha\cos^2\alpha_1}{2Eb[\sin\alpha+(\alpha_2-\alpha)\cos\alpha]-Eb_s(\frac{t_b}{R_{pg}})}d\alpha\\&+\int_{\alpha_{h2}}^{\alpha_2}\frac{1.2(1+v)(\alpha_2-\alpha)\cos\alpha\cos^2\alpha_1}{Eb[\sin\alpha+(\alpha_2-\alpha)\cos\alpha]}d\alpha\end{aligned} \tag{31}$$

$$\begin{aligned}\frac{1}{K_a}=&\int_{-\alpha_1}^{\alpha_{h1}}\frac{(\alpha_2-\alpha)\cos\alpha\sin^2\alpha_1}{2Eb[\sin\alpha+(\alpha_2-\alpha)\cos\alpha]}d\alpha\\&+\int_{\alpha_{h1}}^{\alpha_{h2}}\frac{(\alpha_2-\alpha)\cos\alpha\sin^2\alpha_1}{2Eb[\sin\alpha+(\alpha_2-\alpha)\cos\alpha]-Eb_s(\frac{t_b}{R_{pg}})}d\alpha\\&+\int_{\alpha_{h2}}^{\alpha_2}\frac{(\alpha_2-\alpha)\cos\alpha\sin^2\alpha_1}{2Eb[\sin\alpha+(\alpha_2-\alpha)\cos\alpha]}d\alpha\end{aligned} \tag{32}$$

Finally, for both normal gear and spalling gear, the integrated meshing stiffness of the pinion (subscript 1) and gear (subscript 2) can be written as

$$K_m=1/\left(\frac{1}{K_{b1}}+\frac{1}{K_{s1}}+\frac{1}{K_{a1}}+\frac{1}{K_{f1}}+\frac{1}{K_{b2}}+\frac{1}{K_{s2}}+\frac{1}{K_{a2}}+\frac{1}{K_{f2}}+\frac{1}{K_h}\right) \tag{33}$$

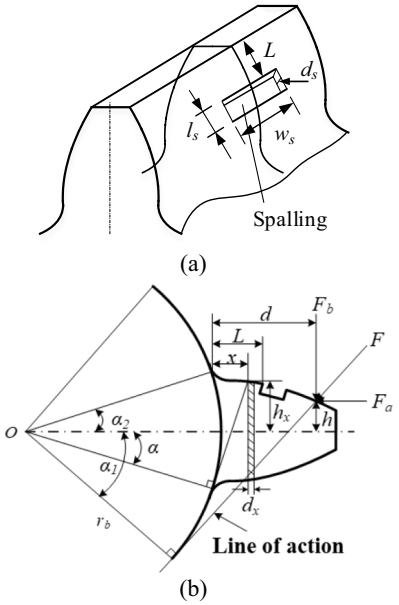

Fig. 3. Schematic diagram of spalling on gear surface: (a) 3D diagram and (b) 2D diagram.

D. SHAFT DEFLECTION AND SHAFT STIFFNESS

Figure 4 shows a simply supported beam model under the action of a concentrated force F. The shaft in the dynamic model is simplified as beam model. The xy plane is the longitudinal symmetry plane of the shaft. Point A and point B are two fulcrum points. Point C is the gear installation position on the shaft, and the gear meshing force is simplified to the concentrated force F. Under the influence of the concentrated force F, the axis will undergo symmetric bending deformation, and the deformed axis will become a deflection line in the xy plane. The displacement of the centroid of the cross-section at x along the y direction is denoted by ω.

The deflection of the beam can be written as [22]

$$\omega=f(x) \tag{34}$$

According to the principle of material mechanics, the deflection along the axis under F can be calculated as

$$f(x)=\begin{cases}-\frac{Fbx}{6El}(l^2-x^2-b^2) & (0\le x\le a)\\ -\frac{Fb}{6El}\left[\frac{l}{b}(x-a)^3+(l^2-b^2)x-x^3\right] & (a\le x\le l)\end{cases} \tag{35}$$

According to definition of stiffness, the bending stiffness of shaft at the position C for gear installation can be obtained as [23]

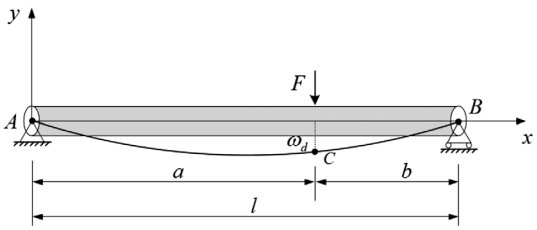

Fig. 4. Simple supported beam model of shaft.

$$K = -\frac{F}{\omega_d} = -\frac{F}{f(x_d)} \tag{36}$$

When the gear is fixed at the middle of the shaft, the stiffness can be written as

$$K_s = \frac{6EIl}{\frac{l}{2}\cdot\frac{l}{2}(l^2-(\frac{l}{2})^2-(\frac{l}{2})^2)} = \frac{48EI}{l^3} = \frac{3E\pi d^4}{4l^3} \tag{37}$$

E. SHAFT CRACK AND SHAFT WHIRLING

Manufacturing errors or assembly errors will lead to reciprocating impact of meshing between gear teeth. Shaft cracks are easy to appear at the installation position of gear under reciprocating impact condition, as shown in Fig. 5.

The magnitude and direction of the stress on the crack surface of the shaft will change with the operation of the shaft. Therefore, the crack on the shaft will present a breathing characteristic, which results in the change of the support stiffness. It is noted that transverse crack is considered in this study. The shaft crack will cause the shaft unbalance and then lead to shaft whirling. The schematic diagram of shaft whirling by shaft crack is shown in Fig. 6.

The switching function $f(\varphi)$ and the cosine wave model are used to simulate the opening and closing process of the shaft crack.

$$f(\varphi) = \frac{[1-\cos(\varphi+\theta+\pi)]}{2} \tag{38}$$

where φ is the angle between the fixed coordinate system and rotor rotation coordinate system, $\varphi = \omega_1 t$. ω_1 is the angular velocity of the pinion, θ is the initial position angle of the shaft crack.

When the shaft crack occurs, the gravity of the gear and the meshing force of the gear teeth will have a transverse impact on one side of the shaft. Therefore, the stiffness of the supporting shaft on both x and y direction will decrease, which can be written as [24]

$$K_{sx} = K_s - f(\varphi)\Delta K_{sx} \tag{39}$$

$$K_{sy} = K_s - f(\varphi)\Delta K_{sy} \tag{40}$$

where $\Delta K_{sx,y}$ means change of the stiffness due to the crack, which is written by

$$\Delta K_{sx} = K_{cx} - K_{ox} \tag{41}$$

$$\Delta K_{sy} = K_{cy} - K_{oy} \tag{42}$$

where $K_{cx,y}$ and $K_{ox,y}$ mean the supporting stiffness of the shaft on x and y direction when the crack is fully closed and open. When crack is fully closed, $K_{cx,y} = K_d$. When crack is fully open, $K_{cx,y}$ can be calculated based on the percentage of inertia moment between crack case (I_{vc}) and normal case (Iv) [24].

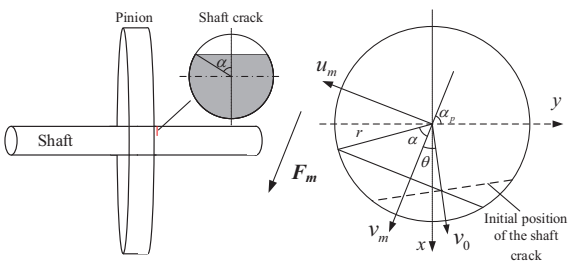

Fig. 5. Diagram of shaft crack.

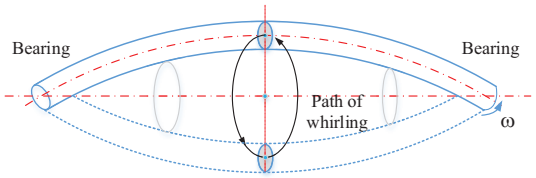

Fig. 6. Diagram of shaft whirling.

The shaft whirling R_w can be calculated from the deflection caused by shaft crack.

$$R_\omega = \Delta\omega = \frac{F}{I_{vo}/I_v \cdot K_d} - \frac{F}{K_d} \tag{43}$$

$$F = mg \times \sin(\alpha_p) + F_m \tag{44}$$

The displacement excitation and its derivative caused by the shaft whirling along the line of action can be given by

$$e_\omega = R_\omega \cos(\omega_\omega t) \tag{45}$$

$$\dot{e}_\omega = -R_\omega\omega_\omega \sin(\omega_\omega t) \tag{46}$$

where R_w is the shaft whirling vector, ω_ω is the whirling frequency, which is equal to rotating frequency in this study.

Under the influences of shaft whirling, the dynamic transmission error δ_{pg} and its differential coefficient v_{pg} can be given as

$$\delta_{pg} = h[(X_g - X_p)\cos\alpha + (Y_p - Y_g)\sin\alpha + r_{bp}\alpha_1 + r_{bg}\alpha_2 - e_\omega] \tag{47}$$

$$v_{pg} = h[(\dot{X}_g - \dot{X}_p)\cos\alpha + (\dot{X}_p - \dot{X}_g)\sin\alpha + r_{bp}\omega_1 + r_{bg}\omega_2 - \dot{e}_\omega] \tag{48}$$

$$h = \begin{cases} 1, & \delta_{pg} > 0 \\ 0, & \delta_{pg} \le 0 \end{cases} \tag{49}$$

where h is a coefficient to judge whether contact occurs between the two-meshing tooth.

III. IMPLEMENTATION OF THE NUMERICAL SIMULATION

A. ASSUMPTIONS AND CONSIDERATIONS

It is noted that the model is established on an ideal working condition, that is, the influence of speed and load fluctuation is neglected. Besides, manufacturing errors, bearing skidding and temperature are also ignored in this model.

B. MAIN PARAMETERS IN NUMERICAL SIMULATION

The main parameters adopted in numerical simulation are recorded in Tables I and II.

Table I. Parameters of the gear and pinion

Parameters	Pinion (*p*)	Gear (*g*)
Teeth number	25	53
Module (*mm*)	3	3
Width (mm)	60	50
Pressure angle (°)	20°	20°
Moment of inertia (kg · m^2)	1.37×10^{-3}	2.31×10^{-2}
Mass (kg)	1.56	5.85

Table II. Parameters of the Bearing6205

Note	Description	Value
M_s	Mass of shaft (kg)	1.3
M_h	Mass of housing (kg)	0.5
M_r	Mass of sensor (kg)	0.02
K_s	Stiffness of shaft (N/m)	2.88×10^9
K_h	Stiffness of housing (N/m)	5.0×10^9
K_r	Stiffness of housing (N/m)	4.0×10^7
C_s	Damping of shaft (Ns/m)	1.23×10^4
C_h	Damping of housing (Ns/m)	3.0×10^4
C_r	Damping of sensor (Ns/m)	357.78

Besides, the shaft rotating speed is 1500 rpm, while the torque provides by the brake is 20 Nm.

C. CHARACTERISTIC FREQUENCIES

Table III displayed the characteristic frequencies of gear and bearing are shown in, containing rotating frequency, GMF, ball pass frequency on inner race (BPFI), ball pass frequency on outer race (BPFO) and cage frequency (CF).

D. FORCE ANALYSIS

In the dynamic model, the time-varying meshing stiffness of the gear pair can be calculated during the model solving by Equation (19). The stiffness and the meshing force are shown in Fig. 7. Note that when there is no external local defect on gear, bearing and shaft, the working condition is named "Baseline."

From Fig. 7, when spalling occurs, the gear meshing stiffness and the dynamic gear meshing force show periodic changes. The stiffness decreases when spalling appears, while the gear meshing force increases. It can be attributed to the excitation of gear local defect on stiffness.

In this model, gear and bearing operate together to transmit motion and power. Therefore, the response of bearing is of great concern. In this part, the load distribution of bearing is analysed. The dynamic resultant force on each ball is shown in Fig. 8.

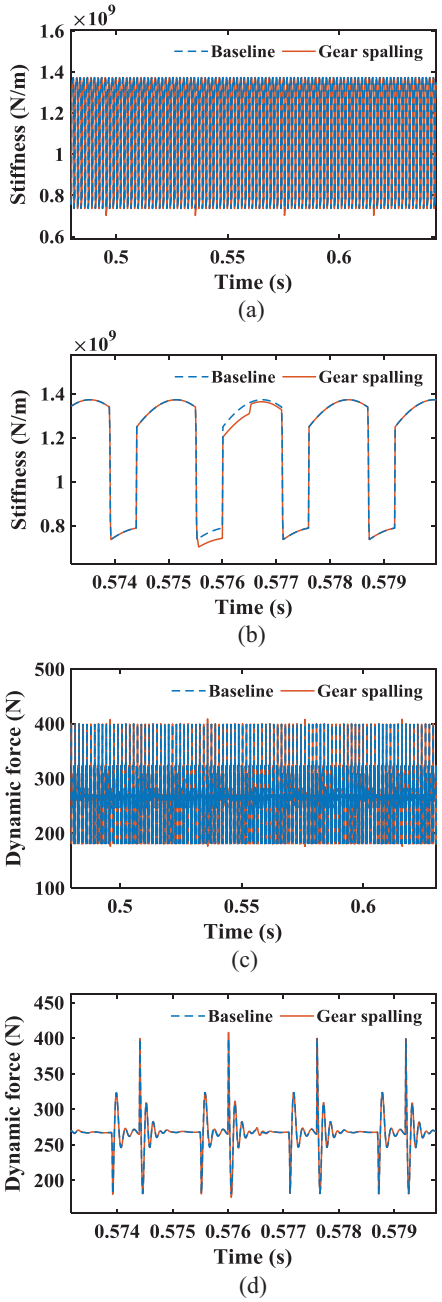

Fig. 7. Force analysis result: (a) gear meshing stiffness, (b) the details of the gear meshing stiffness, (c) gear meshing force and (d) the details of gear meshing force.

From Fig. 8, it finds that the dynamic force on each ball represents periodical waveform, and the nine balls change in turn. This means that with the rotating of the bearing, the dynamic force change with the loaded region and unloaded region, which is consistent with the theoretical load distribution.

Table III. Characteristic frequencies value of bearing and gear

	Rotating frequency			Bearing 1,2		
Rotating speed (rpm)	f_{r1} (Hz)	f_{r2} (Hz)	GMF (Hz)	BPFO	BPFI	CF
1500	25	11.79	625	89.78	135.22	9.98

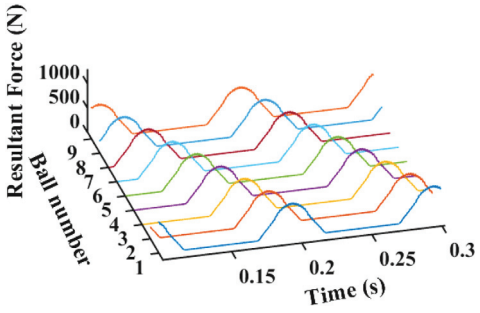

Fig. 8. Dynamic force between raceway and rolling element.

E. VIBRATION RESPONSES UNDER GEAR FAULT

In this section, vibration responses are analysed considering baseline and spalling pinion. The parameter of the spalling is set as $l_s = 2$ mm, $w_s = 20$ mm, $L = 1.8$ mm and $d_s = 1$ mm. Vibration signal of bearing 1 in Fig. 1 is extracted. Analysis from time domain and frequency domain is illustrated in Fig. 9.

As can be seen from Fig. 9(a) and (b), when spalling appears on gear surface, the waveform shows an obvious increase compared with the baseline, and periodic impulses can be recognized from the waveform. As can be seen, periodic impulses with the period of $1/f_{r1}$ can be clearly detected when spalling occurs. After enlargement, periodic impulses with the period of $1/f_m$ are dominant. Through FFT spectrum in Fig. 9(c), the energy of GMF and its harmonics has higher amplitude. After the enlargement of the first-order GMF, the sidebands are located at the both sides of GMF, as shown in Fig. 9(d). The spectrum amplitude of spalling gear shows an obvious increase comparing with the baseline. Figure 9(e) depicts the envelope spectrum. From Fig. 9(e), the amplitude of f_{r1} of spalling gear is much higher than baseline, which verified the modulation phenomenon derived from gear spalling. It means that when gear spalling occurs, the modulation between the gear fault and GMF plays a vital effect.

IV. VIBRATION ANALYSIS UNDER THE INFLUENCE OF SHAFT CRACK

To investigate the vibration features of gear system under the influences of shaft whirling, simulations under baseline and cracked shaft are carried out first. Vibration waveform and spectra of two cases are shown in Fig. 10.

As can be seen from Fig. 10(a) and (b), when crack appears on the shaft, the vibration waveform fluctuates more obvious than baseline. From the FFT spectrum in Fig. 10(c), GMF and its harmonics are dominant. After the enlargement of the first-order GMF, the more sidebands are located at the both sides of GMF when crack occurs, as shown in Fig. 10(d). Through envelope spectrum in Fig. 10(e), the amplitude of f_{r1} of cracked shaft is much higher than baseline, which verified the modulation phenomenon derived from shaft crack.

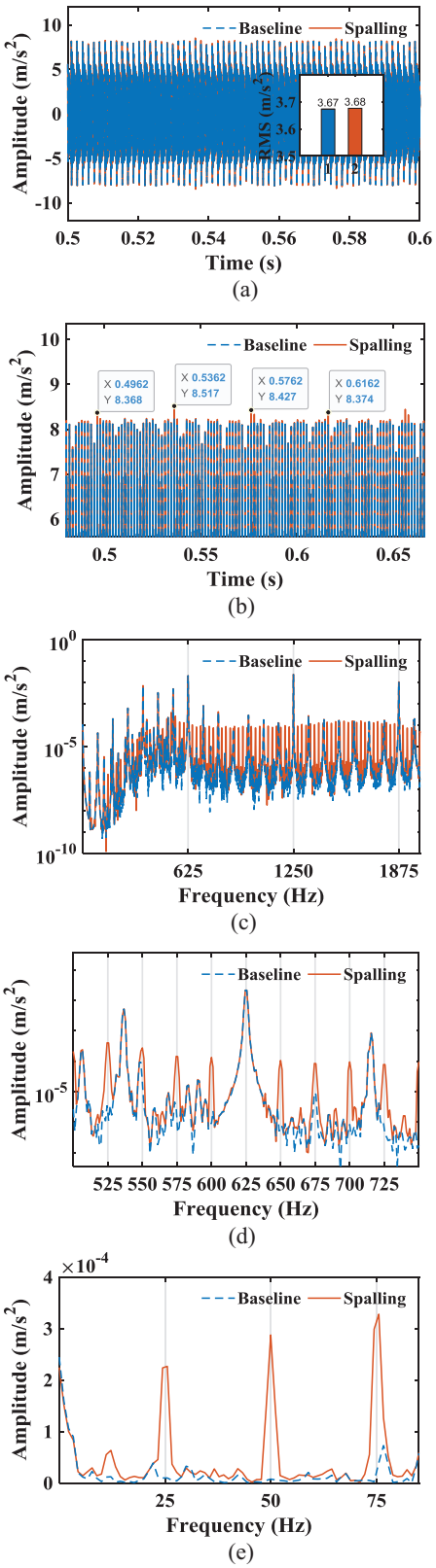

Fig. 9. Comparison of vibration responses between without and with spalling on pinion: (a, b) time domain waveform, (c) FFT spectrum, (d) the enlargement of FFT and (e) envelope spectrum.

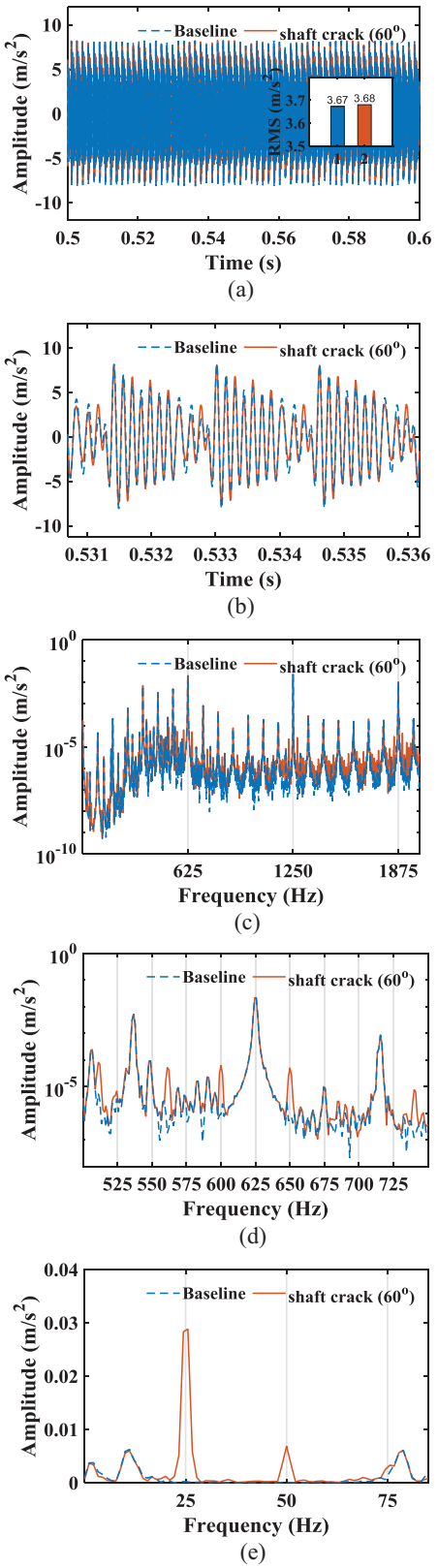

Fig. 10. Result of shaft crack (a) RMS of vibration acceleration and (b) amplitude of rotating frequency of shaft 1 (f_{r1}).

V. EXPERIMENT VERIFICATION

A. EXPERIMENT SETTINGS

A spur-gear gearbox test rig is designed to validate the proposed model. Vibration of the bearing housing was measured through vibration accelerometer. The test rig and measure system are shown in Fig. 11. The gearbox consists of three shafts and two pairs of gear. It is noteworthy that the second pair of gear is utilized to verify the proposed model. The supported bearings are deep grove ball bearing 6205. The tooth number of studied gear pair is 25 and 53, respectively, which is consistent with the dynamic model. During the test, vibration data are acquired under normal gear, gear with spalling and shaft crack. The input rotational speed by the motor is 900 rpm. The load is supplied by the magnetic powder brake and set as 60 Nm.

In order to validate the dynamic model and vibration responses under gear spalling and shaft crack, spalling and crack were machined on gear and shaft, as shown in Fig. 12. As shown in Fig. 12, the spalling is located on the gear surface. The length of the spalling is 2 mm the width of it is 10 mm and the depth of it is 1 mm. In the experiment, the crack circumference angle of the shaft is set as 60°. Besides, the shaft rotating speed is 1200 rpm and the torque provided by the magnetic powder brake is 20 Nm.

Table IV exhibits the characteristic frequencies of the gearbox under speed of 1200 rpm, which contains rotational frequency of shaft and GMF.

Vibration signal of the bearing on drive-end side was measured through accelerometer. Comparison of vibration responses among three cases are made in time domain and frequency domain. Figure 13 exhibits the analysis result of the vibration signal.

As can be seen from Fig. 13(a) and (b), the amplitude of gear spalling and shaft crack is higher than baseline and the impulsive wave is more obvious, which can be attributed to the excitation of the spalling and crack. The amplitude and RMS value are consistent with the simulation.

From the FFT spectrum in Fig. 13(c), spectrum concentrates on around the GMF f_m and its harmonics. It means that GMF extracts more energy during the operations. Sideband can be detected at the both sides of GMF. It can also find that the amplitude of sideband of cracked gear is higher than normal gear.

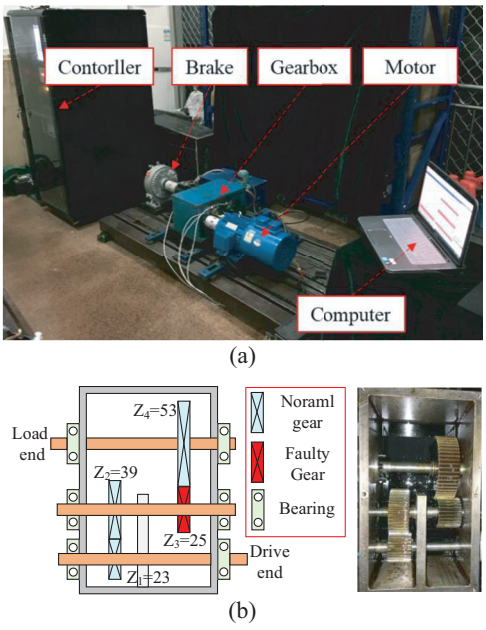

Fig. 11. Test facilities: (a) spur-gear gearbox test rig and (b) the structure of the gearbox.

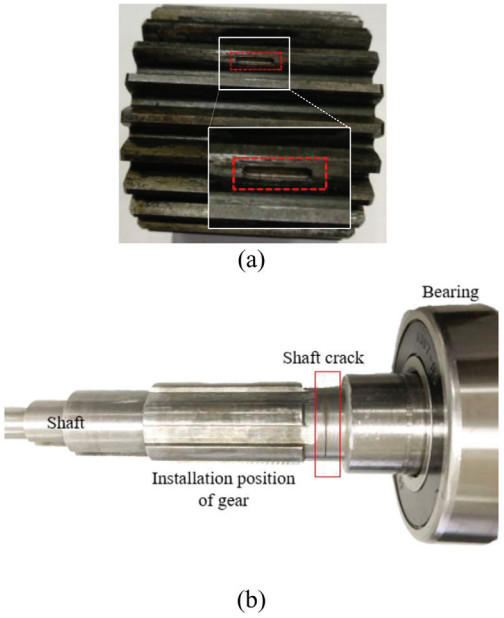

Fig. 12. Gear and shaft used in experiment: (a) spalling gear and (b) cracked shaft.

Table IV. Characteristic frequencies of the gearbox under the speed of 1200 rpm

Description	Value
Rotating speed of the motor (rpm)	1200
Rotating speed of the second shaft (rpm)	707.69
Rotating frequency of the first shaft (Hz)	20
Rotating frequency of the second shaft (Hz)	11.79
Rotating frequency of the second shaft (Hz)	5.56
Gear meshing frequency of first pair	460
Gear meshing frequency of second pair	294.87

The spectrum based on envelope demodulation is exhibited in Fig. 13(d). From Fig. 13(d), the rotating frequency of the second shaft f_r and its harmonics can be clearly detected from the envelope spectrum under three cases. The amplitude of f_r and its harmonics of spalling gear is higher than baseline. It means that when spalling occurs on gear surface, shaft frequency f_r and its harmonics will modulate on the GMF. Note that the fluctuation amplitude on f_r can be attributed to the background noise or assembly error. Even so, the findings of experiment in Fig. 13 and simulation analysis are consistent, which verifies the accuracy of the proposed dynamic model.

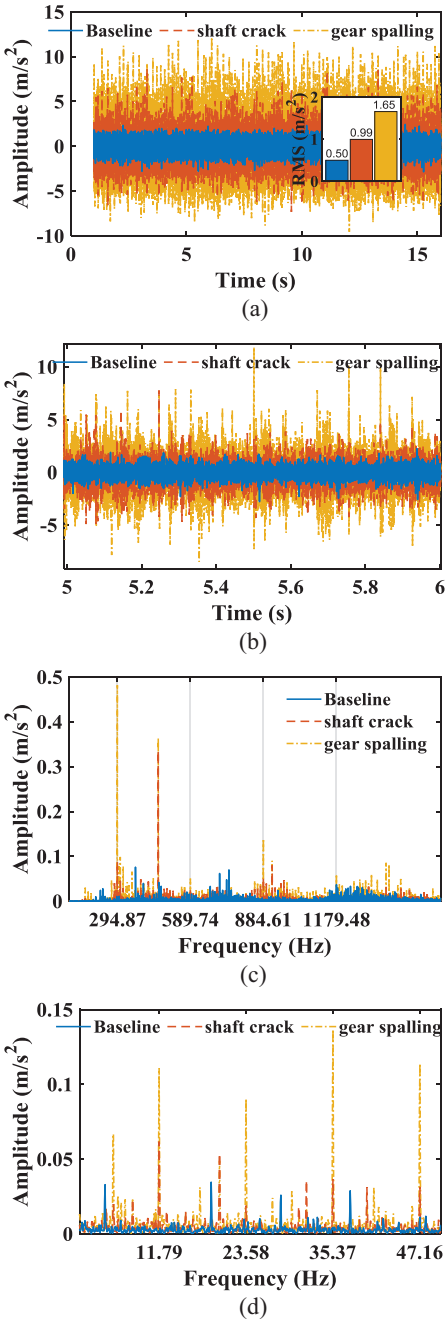

Fig. 13. Comparison of vibration responses: (a) waveform, (b) the enlargement of the waveform, (c) FFT spectrum and (d) envelope spectrum.

VI. COMPREHENSIVE ANALYSIS

A. VIBRATION RESPONSES UNDER THE INFLUENCES OF SPALLING LENGTH AND WIDTH

In this section, force and vibration responses under the influences of different spalling size are exhibited and compared. Figure 14 depicts the comparison on stiffness and dynamic force under different spalling length and width.

As can be seen from Fig. 14, the stiffness decreases with increase in the length and width of the spalling, while the dynamic gear meshing force and vibration signals increase with them. It means that when crack appears on gear tooth root, the stiffness will decrease compared with baseline, which results in the increase of vibration.

RMS of stiffness and vibration and amplitude of rotating frequency of shaft 1, f_{r1}, are calculated under different spalling length and width, as shown in Fig. 15. As can be seen, the RMS of stiffness show downtrend as the increase of spalling length and width, while the RMS and

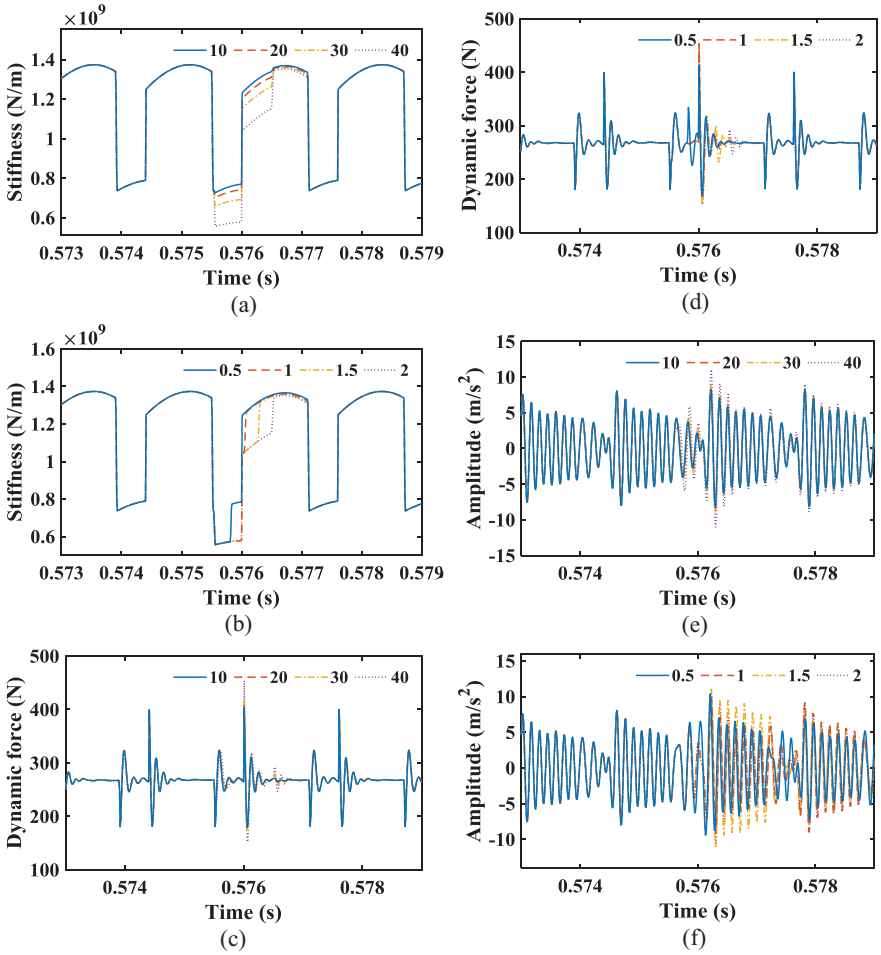

Fig. 14. Comparison result: (a) gear mesh stiffness under different spalling width when the length is 1 mm, (b) gear mesh stiffness under different length when the width is 10 mm, (c) dynamic meshing force under different spalling width when the length is 1 mm, (d) dynamic meshing force under different length when the width is 10 mm, (e, f) vibration waveform under different length and width of the spalling.

the amplitude of f_{r1} of vibration increase by means of the increase of spalling length and width in general. It means that the increase of spalling will result in the increase of vibration. However, the fluctuations can be found in Fig. 15(b) and (c) when spalling length and width change. It means that when spalling size changes, there is a nonlinear relationship between the spalling size and vibration.

B. VIBRATION RESPONSES UNDER THE INFLUENCES OF SHAFT CRACK ANGLE

When the shaft crack angle (α) is set from 0° to 90° with the interval of 10°. 0° means that there is no shaft crack and local fault on gear. Vibration RMS and the amplitude of rotating frequency of shaft 1 (f_{r1}) under different shaft crack angle are shown in Fig. 16.

As can be seen from Fig. 16, the vibration of different shaft cracks shows impulsive waveform. RMS and the amplitude of f_{r1} of vibration increase with the increase of shaft crack angle in general. Similarly, fluctuations can be found in Fig. 16 when the angle is around 30°. However, the total uptrend with the shaft crack angle is obvious.

VII. VIBRATION ANALYSIS UNDER THE INFLUENCE OF SHAFT CRACK AND GEAR FAULT

Vibration under different shaft crack and gear spalling are simulated and analysed. The comparison results are shown in Fig. 17.

As can be seen from Fig. 17, the vibration RMS of different shaft crack and gear spalling shows uptrend. However, the increase of RMS is small. The amplitude of f_{r1} of the vibration acceleration shows different results. As shown in Fig. 17(c), when the spalling size is small, the amplitude of f_{r1} shows uptrend with the shaft crack angles. When the spalling width is 40 mm, amplitude of f_{r1} fluctuates. It means that, when larger spalling appears with lager width, the amplitude of characteristic frequency f_{r1} will not show obvious increase with shaft crack angles, which is different with the result in Fig. 16. Similarly, when the shaft crack is larger, including 50°, 60°, 70°, 80° and 90°, the amplitude of frequency f_{r1} decrease with the spalling width. It means that when gear spalling and shaft crack appear, the vibration is complex and nonlinear.

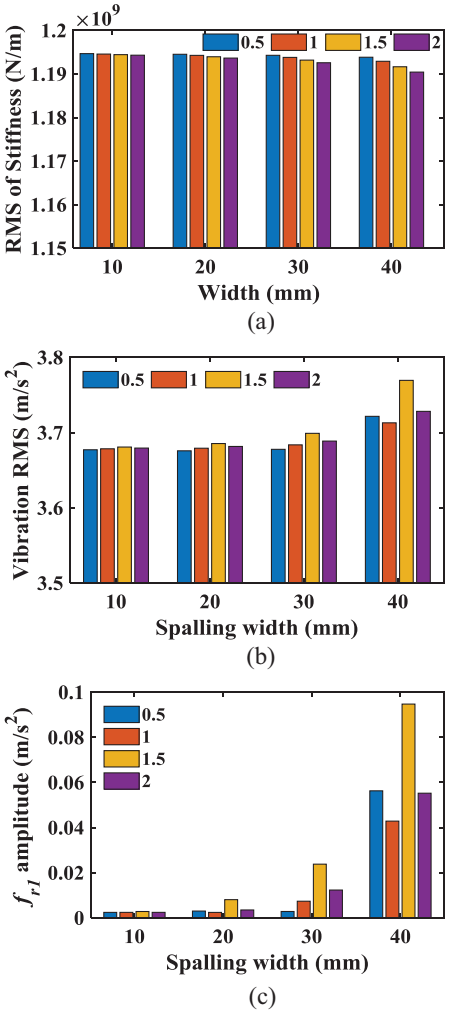

Fig. 15. Comparison of stiffness and vibration under different length and angle: (a) RMS of stiffness, (b) RMS of vibration signals and (c) amplitude of f_{r1}.

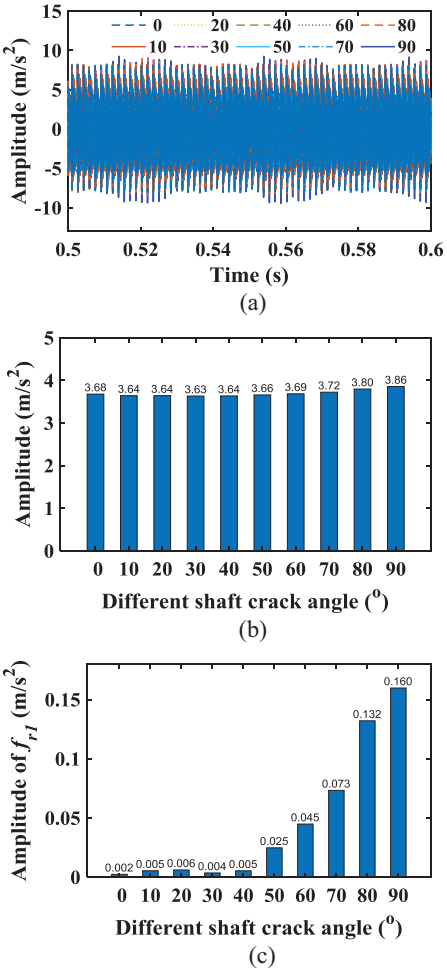

Fig. 16. Result of shaft crack: (a) vibration signal, (b) RMS of vibration acceleration and (c) amplitude of rotating frequency of shaft 1 (f_{r1}).

VIII. DISCUSSION

Through the proposed dynamic model, vibration characteristics considering local defects on gear and shaft are investigated. From the result, RMS and the amplitude of shaft rotating frequency will fluctuate or increase nonlinearly when gear spalling size and shaft crack angle is larger. Therefore, it is not perfectly reasonable to monitor it from the single modulation frequency. It leads to difficulty for the fault diagnosis of gearbox, and it should take care when gear spalling and shaft crack deteriorate. It is necessary to find new indicators for detection. Even so, the establishment of such a model can provide theoretical foundation for gearbox fault diagnosis. The model can be used to simulate vibration of gearbox system to study the vibration characteristics under local defects. Besides, the model has some limitations on applications. The structure of the model is assumed to be symmetrical. Geometry and assembly errors, such as misalignment, are ignored in this model. Besides, lubrication, temperature and bearing skidding are also ignored in this model. Therefore, there are several potential avenues for improving the proposed model. The influence of shaft whirling and bearing clearances on the time-varying stiffness of gear meshing is one of the future works, especially when the system is not symmetrical. Study on the dynamic characteristics of shaft and bearing on time-vary gear mesh stiffness is one of the future works.

IX. CONCLUSIONS

This study investigates a gear-shaft-bearing-housing vibration model considering the interaction between gear and bearing, as well as shaft whirling. Vibration response analysis is carried out based on the model under the effect of gear spalling and shaft crack. Through numerical and experimental analysis, the key findings and the conclusions can be drawn as

1. The proposed coupled dynamic model exhibits better performance on revealing the mechanism in the gear-shaft-bearing system.
2. Based on the spectrum, GMF is dominant in the gearbox system. When local defects appear on gear surfaces or shaft, sidebands can be detected on both sides of GMF and its harmonics.
3. With the increase of spalling size, RMS of stiffness show downtrend, resulting in the increase of vibration level, including the vibration RMS and the amplitude of first three order rotating frequency. It means that the

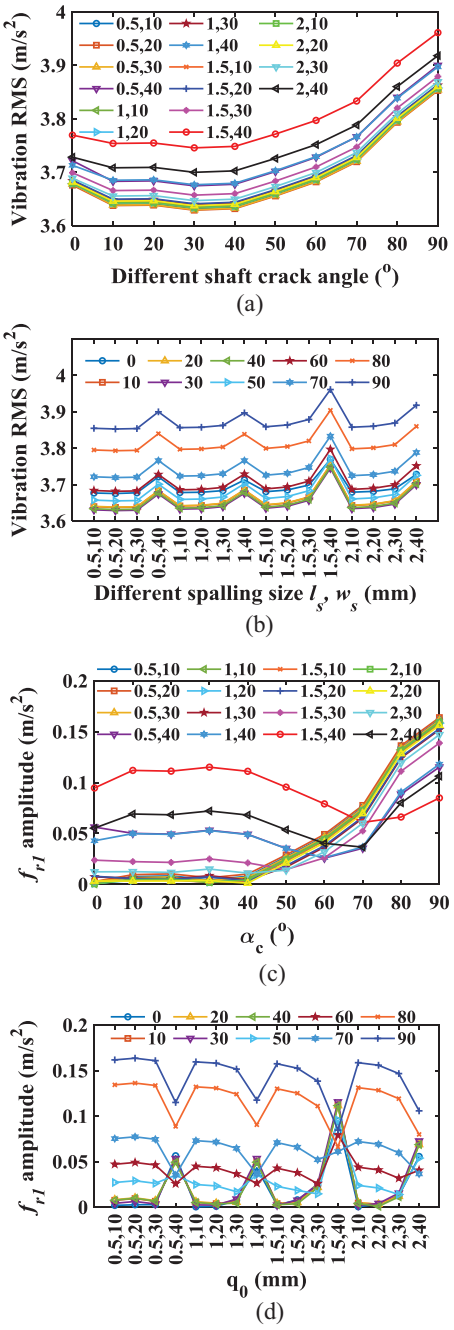

Fig. 17. Comprehensive result under different shaft crack angle and gear fault (a) RMS under different shaft crack angle, (b) RMS under different gear fault, (c) fr1 under different shaft crack angle and (d) f_{r1} under different gear fault.

growth of spalling will result in the increase of vibration and modulation.

4. An experiment was designed to certify the proposed dynamic model based on spur-gear gearbox test rig. Experiment analysis and simulation result are consistent with vibration responses under the effect of gear spalling and shaft crack, which demonstrated the rationality of the enriched gear-shaft-bearing dynamic model.
5. Comprehensive vibration analysis under different gear spalling and shaft crack shows that when gear spalling size and shaft crack angle are small, RMS and the amplitude of shaft rotating frequency have better linear growth, while fluctuations or downtrend will occur when gear spalling size and shaft crack angle is larger.

ACKNOWLEDGMENTS

This work was supported by National Key R&D Program of China (No. 2022YFB3303600) and the Fundamental Research Funds for the Central Universities (No. 2022CDJKYJH048).

CONFLICT OF INTEREST STATEMENT

The authors declare no conflicts of interest.

REFERENCES

[1] R. Randall, "Detection and diagnosis of incipient bearing failure in helicopter gearboxes," *Eng. Fail. Anal.*, vol. 11, no. 2, pp. 177–190, 2004.

[2] R. Zhang, J. X. Gu, and F. Gu, "Gear wear process monitoring using a sideband estimator based on modulation signal bispectrum," *Appl. Sci.*, vol. 7, no. 3, p. 274, 2017.

[3] R. Zhang, F. Gu, and H. Mansaf, "Gear wear monitoring by modulation signal bispectrum based on motor current signal analysis," *Mech. Syst. Sig. Process.*, vol. 94, pp. 202–213, 2017.

[4] M. Xu, G. Feng, and Q. He, "Vibration characteristics of rolling element bearings with different radial clearances for condition monitoring of wind turbine," *Appl. Sci.*, vol. 10, p. 4731, 2020.

[5] H. Ma, R. Song, X. Pang, and B. Wen, "Time-varying mesh stiffness calculation of cracked spur gears," *Eng. Fail. Anal.*, vol. 44, pp. 179–194, 2014.

[6] H. Ma, J. Zeng, R. Feng, X. Pang, Q. Wang, and B. Wen, "Review on dynamics of cracked gear systems," *Eng. Fail. Anal.*, vol. 55, pp. 224–245, 2015.

[7] Z. Chen and Y. Shao, "Dynamic simulation of spur gear with tooth root crack propagating along tooth width and crack depth," *Eng. Fail. Anal.*, vol. 18, no. 8, pp. 2149–2164, 2011.

[8] Z. Chen and Y. Shao, "Mesh stiffness calculation of a spur gear pair with tooth profile modification and tooth root crack," *Mech. Mach. Theory*, vol. 62, pp. 63–74, 2013.

[9] Z. Chen, W. Zhai, and K. Wang, "Vibration feature evolution of locomotive with tooth root crack propagation of gear transmission system," *Mech. Syst. Signal Process.*, vol. 115, pp. 29–44, 2019.

[10] L. Wang and Y. Shao, "Fault mode analysis and detection for gear tooth crack during its propagating process based on dynamic simulation method," *Eng. Fail. Anal.*, vol. 71, pp. 166–178, 2017.

[11] N. Sawalhi and R. Randall, "Simulating gear and bearing interactions in the presence of faults–Part I: the combined gear bearing dynamic model and the simulation of localised bearing faults," *Mech. Syst. Sig. Process.*, vol. 22, pp. 1924–1951, 2008.

[12] N. Sawalhi and R. Randall, "Simulating gear and bearing interactions in the presence of faults–Part II: simulation of the vibrations produced by extended bearing faults," *Mech. Syst. Sig. Process.*, vol. 22, 1952–1966, 2008.

[13] W. Zeng, X. Zhu, and Z. Wei, "Study on nonlinear dynamic response of the gear-shaft-housing coupling system," *Appl. Mech. Mater.*, vol. 26–28, pp. 805–808, 2010.

[14] Z. Hu, J. Tang, and J. Zhong, "Effects of tooth profile modification on dynamic responses of a high speed gear-rotor-bearing system," *Mech. Syst. Sig. Process.*, vol. 76–77, pp. 294–318, 2016.

[15] H. Xiao, X. Zhou, and J. Liu, "Vibration transmission and energy dissipation through the gear-shaft-bearing-housing system subjected to impulse force on gear," *Measurement*, vol. 102, pp. 64–79, 2017.

[16] A. Fernandez-Del-Rincon, P. Garcia, and A. Diez-Ibarbia, "Enhanced model of gear transmission dynamics for condition monitoring applications: effects of torque, friction and bearing clearance," *Mech. Syst. Sig. Process.*, vol. 85, pp. 445–467, 2017.

[17] Y. Chen, T. Yang, and S. Choi, "Dynamic analysis of a double-helical geared rotor system with oil-film bearing," *Aircr. Eng. Aerosp. Tec.*, vol. 92, pp. 653–662, 2020.

[18] M. Xu, Y. Han, X. Sun, Y. Shao, F. Gu, and B. Andrew, "Vibration characteristics and condition monitoring of internal radial clearance within a ball bearing in a gear-shaft-bearing system," *Mech. Syst. Signal Process.*, vol. 1, p. 108280, 2022.

[19] M. Xu, Z. Song, X. Ding, G. Li, Y. Shao, and J. X. Gu, "An improved dynamic modelling for exploring ball bearing vibrations from time-varying oil film," *J. Dyn. Monit. Diagnost.*, pp. 93–102, 2022.

[20] Z. Cao, Y. Shao, M. Rao, and W. Yu, "Effects of the gear eccentricities on the dynamic performance of a planetary gear set," *Nonlinear. Dyn.*, vol. 91, no. 1, pp. 1–15, 2018.

[21] S. Wu, M. J. Zuo, and A. Parey, "Simulation of spur gear dynamics and estimation of fault growth," *J. Sound Vib.*, vol. 317, no. 3–5, pp. 608–624, 2008.

[22] N. A. Saeed, "On the steady-state forward and backward whirling motion of asymmetric nonlinear rotor system," *Euro. J. Mech.-A/Solids*, vol. 80, p. 103878, 2020.

[23] J. Lei, R. Zhou, H. Chen, Y. Gao, G. Lai, "Experimental investigation of effects of ship propulsion shafting alignment on shafting whirling and bearing vibrations," *J. Marine Sci. Tech.*, vol. 27, no. 1, pp.151–162, 2022.

[24] X. Zhang, Y. Yang, M. Shi, A. Ming, and P. Wang, "Novel energy identification method for shallow cracked rotor system," *Mech. Syst. Sig. Process.*, vol. 186, p. 109886, 2023.